Biophysical *Journal*
Article

Biophysical Society

Physical phenotype of blood cells is altered in COVID-19

Markéta Kubánková,[1] Bettina Hohberger,[2] Jakob Hoffmanns,[2] Julia Fürst,[3] Martin Herrmann,[4,5] Jochen Guck,[1,6,*] and Martin Kräter[1]

[1]Max Planck Institute for the Science of Light & Max-Planck-Zentrum für Physik und Medizin, Erlangen, Germany; [2]Department of Ophthalmology, Friedrich-Alexander-University Erlangen-Nürnberg, Erlangen, Germany; [3]Department of Internal Medicine 1 and [4]Department of Internal Medicine 3, University Medical Center Erlangen, Friedrich-Alexander-University Erlangen-Nürnberg, Erlangen, Germany; [5]Deutsches Zentrum Immuntherapie, Erlangen, Germany; and [6]Department of Physics, Friedrich-Alexander-University Erlangen-Nürnberg, Erlangen, Germany

ABSTRACT Clinical syndrome coronavirus disease 2019 (COVID-19) induced by severe acute respiratory syndrome coronavirus 2 is characterized by rapid spreading and high mortality worldwide. Although the pathology is not yet fully understood, hyperinflammatory response and coagulation disorders leading to congestions of microvessels are considered to be key drivers of the still-increasing death toll. Until now, physical changes of blood cells have not been considered to play a role in COVID-19 related vascular occlusion and organ damage. Here, we report an evaluation of multiple physical parameters including the mechanical features of five frequent blood cell types, namely erythrocytes, lymphocytes, monocytes, neutrophils, and eosinophils. More than four million blood cells of 17 COVID-19 patients at different levels of severity, 24 volunteers free from infectious or inflammatory diseases, and 14 recovered COVID-19 patients were analyzed. We found significant changes in lymphocyte stiffness, monocyte size, neutrophil size and deformability, and heterogeneity of erythrocyte deformation and size. Although some of these changes recovered to normal values after hospitalization, others persisted for months after hospital discharge, evidencing the long-term imprint of COVID-19 on the body.

SIGNIFICANCE Coronavirus disease 2019 (COVID-19) can lead to the impairment of the circulatory system, including effects such as vascular occlusion and hypoxemia. The physical properties of blood cells have crucial roles for proper circulation. A quick and simple examination of these properties would accomplish an unmet clinical need for rapid diagnostics of the cell's functional status. Here, we employed real-time deformability cytometry—a label-free, high-throughput imaging technology—to assess various physical properties of blood cells. We identified significant and persisting changes of cell size and mechanical properties in acute-phase and post-COVID-19. These changes might be predictive for cell functionality such as oxygen delivery. Thus, our findings have implications for COVID-19 diagnostics and treatment.

INTRODUCTION

Peripheral blood is a key body fluid analyzed during the diagnostic routine, including infectious disease diagnostics. Infection by severe acute respiratory syndrome coronavirus 2 (SARS-CoV-2) may lead to the clinical syndrome coronavirus disease 2019 (COVID-19), which is accompanied by changes in numbers and phenotypes of blood cells (1). Typically, various immune cells such as T lymphocytes, monocytes, and macrophages get activated and contribute to the so-called hyperinflammatory response (2). The uncontrolled inflammation is believed to be a major cause of disease severity and death during COVID-19 (3). Furthermore, abnormal coagulation and thrombotic events leading to vascular occlusion are described as major contributors to the high mortality (4,5).

Apart from the biochemical state of blood cells, infectious diseases can also alter their physical properties, including morphological or mechanical features. It has long been known that mechanical properties of cells can act as a disease marker, as reviewed by Di Carlo (6), and can contribute to vascular occlusion, as reviewed by Lipowsky (7). To date, a systematic evaluation of the effect of COVID-19 on the physical phenotypes of the most

Submitted December 15, 2020, and accepted for publication May 27, 2021.

*Correspondence: jochen.guck@mpl.mpg.de

Editor: Paul A. Janmey.

https://doi.org/10.1016/j.bpj.2021.05.025

frequent blood cells was missing. To address this gap, we employed real-time deformability cytometry (RT-DC), a label-free, high-throughput technology that allows quick image-based mechanical interrogation of cells at rates of up to 1000 cells per second (8). Previously, the technique was used to detect disease specific signatures of blood cell pathological changes in several conditions, including spherocytosis, malaria, acute lymphoid leukemia, and acute myeloid leukemia (9). During viral respiratory tract infection, Toepfner et al. (9) reported an increase of neutrophil and monocyte size and deformability, as well as larger and more deformable lymphocytes in acute Epstein-Barr-virus (EBV) infection.

Here, we examine COVID-19 related changes of physical phenotype of several cell types found in peripheral blood, namely erythrocytes, lymphocytes, monocytes, and neutrophils. In total, more than 4×10^6 blood cells from 55 blood samples were analyzed, including 17 COVID-19 positive patients, 14 recovered patients, and 24 age-matched volunteers showing no indication of infection or inflammatory disease. We found that COVID-19 is linked with significantly decreased lymphocyte stiffness, increased monocyte cell size, the appearance of smaller and less deformable erythrocytes, and the presence of large, deformable, activated neutrophils. Certain changes had not returned to the control group levels months after release from the hospital, bringing evidence of the long-lasting effects of COVID-19 on the circulatory system.

Our results show that RT-DC can be used to follow the course of COVID-19 and the immune response against it. In the future, we anticipate that measurements of morphological and mechanical properties of blood cells will contribute toward improving infectious disease diagnostics.

MATERIALS AND METHODS

Peripheral blood collection

COVID-19 patients were hospitalized with a majority at the intensive care unit of the Department of Internal Medicine 1, Friedrich-Alexander-University Erlangen-Nürnberg, Germany (FAU) showing different severity levels at the time of blood sampling. COVID-19 venous blood samples (n = 17) were taken from hospitalized patients of the Department of Internal Medicine 1, FAU, between April and May 2020. Recovered patient venous blood samples (n = 14) were taken from patients of the Department of Internal Medicine 1, FAU, in recovery from COVID-19 between 4 and 8 months after release from the hospital (median 7.1 ± 1.1 months). All patients had positive PCR tests for COVID-19. Control venous blood samples (healthy cohort) were taken from patients of the Department of Ophthalmology, FAU (patient information can be found in Table S1). Blood was drawn using a 20-gauge multifly needle into a sodium citrate S-monovette by vacuum aspiration with the tenets of the Declaration of Helsinki. Informed written consent was obtained from all participants. All experiments were performed according to the institutional guidelines and the ethical approval of the Ethical Committee of the University Medical Center of Erlangen (permits #193_13B, #174_20B, and #295_20B). After blood collection, samples were used for clinical routine diagnostics, and an aliquot was taken for RT-DC analysis within the standard storing time and conditions.

Sample preparation

Before measurement, 50 μL of whole blood was gently mixed with 950 μL of measurement buffer composed of 0.6% (m/v) methyl cellulose dissolved in phosphate-buffered saline (Fig. 1), adjusted to a viscosity of 60 mPa s at 24°C using a falling ball viscometer (Haake; Thermo Fisher Scientific, Waltham, MA).

RT-DC

RT-DC measurements were performed as described previously using an AcCellerator instrument (Zellmechanik Dresden, Dresden, Germany) (9). The cell suspension was loaded into a 1 mL syringe attached to a syringe pump (neMESYS; Cetoni, Korbußen, Germany) and connected by PEEK-tubing (IDEX Health & Science, Middleboro, MA) to a microfluidic chip made of polydimethylsiloxane (PDMS) bonded on cover glass. A second syringe with sheath fluid (pure measurement buffer) was connected to the chip, which consisted of two inlets (one for the sheath fluid and one for the sample) and one outlet connected by a channel constriction of 20 × 20 μm square cross section, where the measurement was performed. The total flow rate was 0.06 μL/s, of which the sheath flow rate was 0.045 μL/s and the sample flow rate was 0.015 μL/s. To perform a measurement, the chip was mounted on the stage of an inverted high-speed microscope equipped with a complementary metal-oxide semiconductor (CMOS) camera. Measurement temperature was 23°C. Images were acquired at a frame rate of 1600 fps. Cells were detected in a region of interest of 250 × 80 pixels, and morphological and mechanical parameters were acquired in real time (Fig. 1).

Data analysis

Cell images were analyzed using ShapeOut software (10) and Python 3.7 using dclab library (11). For each patient, the five studied cell populations were hand gated in the cell brightness-area parameter plot according to the procedure described in Toepfner et al. (9). We applied a gate for minimal cross-sectional area (15 μm^2) and for the area ratio (1–1.05 for leukocytes, 1–1.08 for erythrocytes). The calculation of deformation, a measure of how much the cell shape deviates from circularity, was obtained from the image using the projected area (A) and cell contour length calculated from the convex hull (l):

$$Deformation = \frac{1 - 2\sqrt{\pi A}}{l}. \quad (1)$$

The calculation of the Young's modulus was done using a look-up table derived from simulations based on the finite elements method (12) and the analytical solution (13). Cell volume was computed from the event contour under the assumption of rotational symmetry with a rotational axis parallel to the flow direction. The calculation is based on a full rotation of the upper and the lower halves of the contour, which are then averaged.

Statistical analysis was done in Python 3.7 using Kruskal-Wallis H-test and post hoc Dunn's test with Bonferroni correction. In graphs, p-values are represented by $*p < 0.05$, $**p < 0.01$, and $***p < 0.001$. The effect size was estimated by ϵ^2 (14), which was calculated from the H-test statistic as follows (15):

$$\epsilon_R^2 = \frac{H}{(n^2 - 1)/(n + 1)}, \quad (2)$$

where H is the Kruskal-Wallis H-test statistic, n is the total number of observations, and the ϵ^2 coefficient assumes the value from 0 (indicating no relationship) to 1 (perfect relationship). The effect size was interpreted according to Rea and Parker (16); details are found in Table S2.

For the comparison of three donors at two time points (during and post-COVID-19), statistical analyses were carried out using a one-dimensional

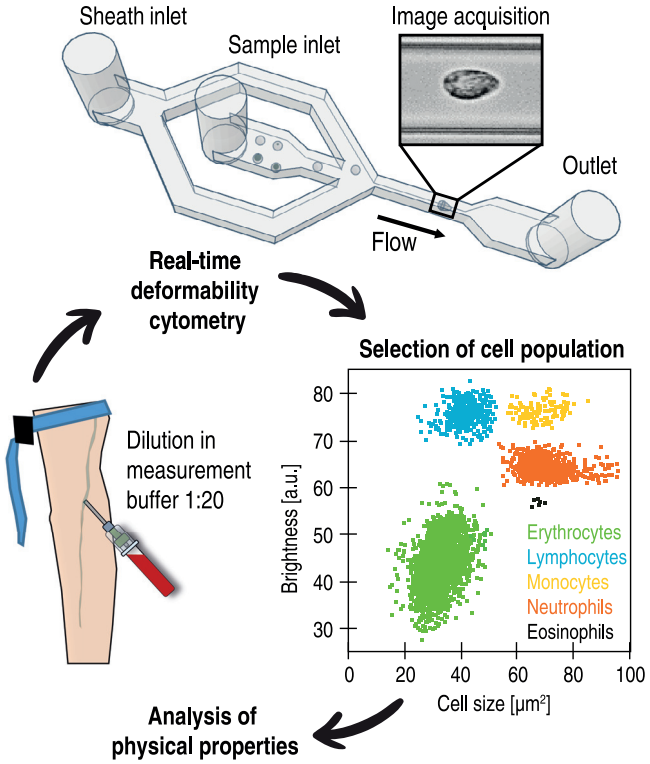

FIGURE 1 Scheme of an RT-DC measurement of a peripheral blood sample. 50 μL of venous citrate-anticoagulated blood is diluted and mixed gently in 950 μL of measurement buffer consisting of phosphate-buffered saline and methyl cellulose. The blood cell suspension is pumped through a microfluidic chip mounted on an inverted microscope, and single-cell images are processed in real time to obtain the physical parameters of each cell. During postprocessing, cell populations of interest are manually gated according to brightness, and the physical properties of each population are analyzed.

linear mixed model that incorporates fixed effect parameters and random effects to analyze differences between cell subsets and replicate variances, respectively. p-values were determined by a likelihood ratio test, comparing the full model with a model lacking the fixed effect term (17), and are represented in the graphs by $*p < 0.05$, $**p < 0.01$, and $***p < 0.001$.

Data availability statement

All data acquired and used for analysis are publicly available. Zenodo.org: 10.5281/zenodo.4737521.

RESULTS

We studied the peripheral blood from 17 COVID-19 patients hospitalized at the time of sample collection (median age 68 $\pm$ 10.4 years) compared with a cohort of 24 volunteers free from infectious or inflammatory diseases (62.5 $\pm$ 13.6 years) and 14 blood donors on average 7 months after hospitalization with COVID-19 (age 58.6 $\pm$ 12.4 years, herein referred to as the "recovered" patients). Whole blood was diluted in measurement buffer at a ratio of 1:20 and analyzed with RT-DC (Fig. 1). For each patient, the five most frequent blood cell populations were manually gated according to the established analysis protocol (9): erythrocytes, lymphocytes, monocytes, neutrophils, and eosinophils.

In agreement with other studies (18,19) we observed significant alterations of white blood cell counts in severe COVID-19 cases, namely neutrophilia (elevated number of neutrophils) and lymphopenia (decreased number of lymphocytes) (Fig. S1). Here, it should be noted that reports of lymphopenia in literature are controversial, as, for instance, Woodruff et al. (20) reported elevated levels of lymphocytes in COVID-19 patients. The median neutrophil/lymphocyte ratio (NLR) increased from 0.97 $\pm$ 0.70 to 3.62 $\pm$ 3.36, with several cases in which NLR was over 8. The NLR increase calculated from RT-DC data was consistent with literature, in which NLR is reported as a prognostic marker of COVID-19 mortality (21). In some patients, we also observed monocytosis (22); whereas the proportion of monocytes/total white blood cells was mostly in the normal range of 2–8%, in several COVID-19 cases it reached over 10% (Fig. S1). No significant changes were found in eosinophil counts. Overall, these findings confirm that, purely from the images of cells obtained with RT-DC, it is possible to reproduce the results of conventional complete blood counts (9). The focus of this study, however, was the interrogation of changes of blood cell physical phenotype. The following sections describe alterations of erythrocytes and leukocytes during COVID-19. Although the most striking findings are presented below, the reader will find a comprehensive overview of all the analyzed physical features for each cell type in Figs. S2–S6.

COVID-19 induces the appearance of erythrocytes with distinct physical phenotype

RT-DC analysis revealed erythrocyte anomaly in COVID-19 patients, mainly characterized by the appearance of small erythrocytes with low deformation in standardized channel flow conditions (Fig. 2, *A–E*). The median deformation of erythrocytes exhibited a weak decrease in COVID-19 patients compared with healthy donors and recovered patients (Kruskal-Wallis $p = 0.22$, $\chi^2 = 3.1$, $\varepsilon^2 = 0.06$) (Fig. 2 *F*). It is noteworthy that several of the COVID-19 patients had very low median erythrocyte deformability compared with the rest of the blood donors.

Significant differences with strong effect size were observed in the standard deviation (SD) of erythrocyte deformation (Kruskal-Wallis $p < 0.0001$, $\chi^2 = 42.3$, $\varepsilon^2 = 0.78$) (Fig. 2 *G*). The significant broadening of the deformation distribution during COVID-19 was the result of the appearance of erythrocytes with low deformation, as shown in Fig. 2 *D*. Such cells were rare in the healthy patient cohort.

Alongside the significant difference in SD of deformation between hospitalized patients and the healthy cohort ($p <$ 0.0001; see Table S2 for detailed results of Dunn's post

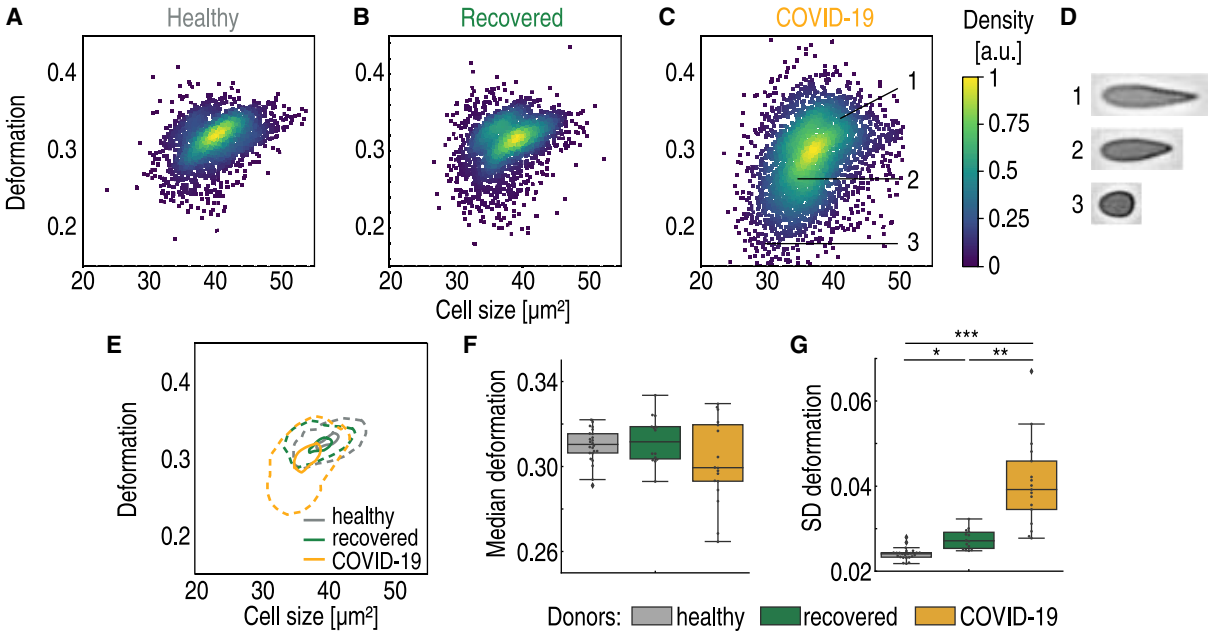

FIGURE 2 Decreased size and deformability of erythrocytes of hospitalized COVID-19 patients. Typical scatter plot of erythrocyte deformation versus cell size (cross-sectional area) of a healthy blood donor with no known viral infection (*A*) compared with a patient 4 months after undergoing COVID-19 (*B*) and a patient with COVID-19 in an intensive care unit (*C*) is given. The erythrocytes shown in (*D*) are representative images of cells in the clusters marked by corresponding numbers in the scatter plot. (*E*) Kernel density estimate plots demonstrating the differences in cell size and deformation between the three donors (*A–C*). The comparison of median values of deformation (*F*) and SD of deformation (*G*) between the control group of blood donors (n = 24), recovered patients (n = 14), and patients hospitalized with COVID-19 (n = 17) is shown. Statistical comparisons were done using Kruskal-Wallis test with Dunn's post hoc test; $*p < 0.05$, $**p < 0.01$, $***p < 0.001$.

hoc tests), we also found significant differences between the recovered and hospitalized cohorts ($p = 0.002$) and between the recovered and healthy cohorts ($p = 0.03$) (Fig. 2 *G*). Clearly, erythrocytes of the recovered patients had not fully returned to the state of the healthy cohort.

In addition to the increased SD of deformation, we also found increased SD of cell size, specifically the cross-sectional area of the image-derived cell contours and the cell volume (Fig. S2). The increased SDs of cell size and deformation were in accordance with reported broadening of the red blood cell distribution width, a routine complete blood count component (23). Some of the cells were not only smaller than usual but also asymmetrically shaped, raising suspicion of the presence of fragmented erythrocytes. This is a valid hypothesis, as schistocytes have been reported as a marker of severe COVID-19 (24).

In general, the phenotype changes observed with RT-DC may be associated with structural and functional changes. A recent study has reported that COVID-19 causes irreversible damage to the erythrocyte proteome (25). The authors found that oxidative stress connected with COVID-19 damages essential proteins in erythrocytes, including those that influence membrane structure and the ability to transport and deliver oxygen. Because mature erythrocytes cannot synthesize new proteins to replace damaged ones and the average lifespan of erythrocytes is 120 days, the authors hypothesize that the circulation of irreversibly damaged erythrocytes with impaired function could contribute to the long-term effects of COVID-19 (25).

According to our findings, COVID-19 is connected with the appearance of less deformable erythrocytes. Cell deformability is thought to be a key factor determining splenic clearance (26), and it is likely that erythrocytes strongly deviating from normal deformability get removed by the spleen. Interestingly, we observed that erythrocyte heterogeneity in recovered patients had not fully decreased back to healthy donor levels. Thus, we hypothesize that erythrocytes with only minor deviations from normal deformability pass through the spleen unnoticed. Because of the long erythrocyte lifespan, such cells may remain in the blood circulation for months. The altered physical properties of circulating blood cells could even induce mechanical stress and impair the function of the spleen in filtering out abnormal red blood cells. These phenomena could contribute to the long-term problems experienced by many COVID-19 patients (27).

Decreased lymphocyte stiffness in COVID-19 patients

RT-DC analysis revealed increased deformability of peripheral blood lymphocytes during severe COVID-19 ($p = 0.013$, $\chi^2 = 8.7$, with relatively strong effect size $\varepsilon^2 = 0.16$), as can be seen in Fig. 3, *A–E*. Although lymphocyte

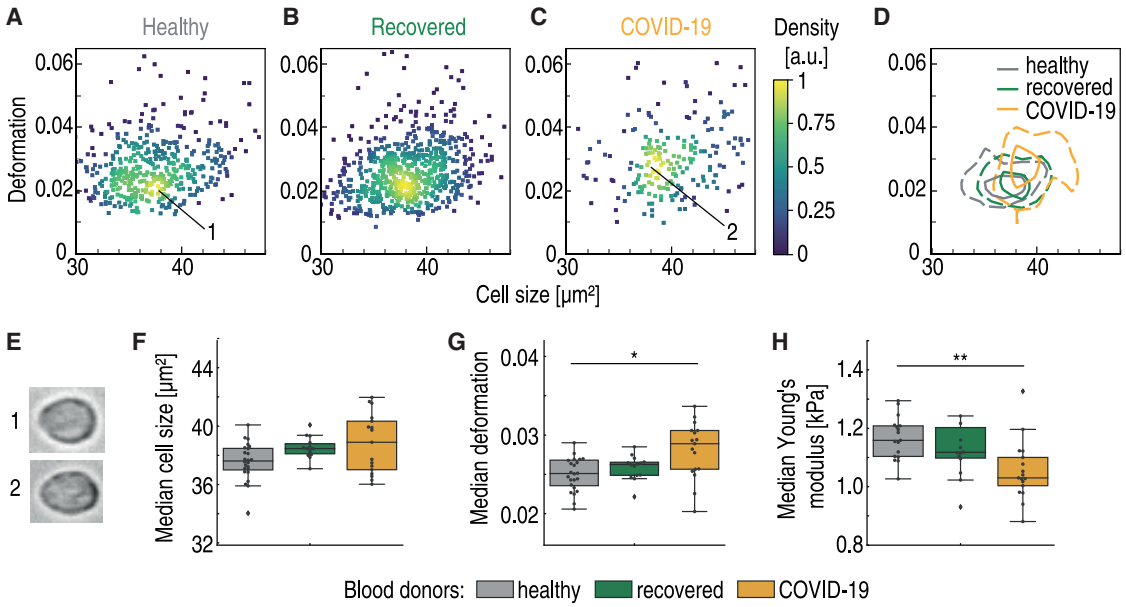

FIGURE 3 Lymphocytes are less stiff in peripheral blood of hospitalized COVID-19 patients. Typical scatter plot of lymphocyte deformation versus cell size (cross-sectional area) of a healthy blood donor with no known viral infection (*A*) compared with a patient 4 months after undergoing COVID-19 (*B*) and a patient with COVID-19 in an intensive care unit (*C*) is given. (*D*) Kernel density estimate plots demonstrating the differences in cell size and deformation among the three donors (*A–C*). (*E*) Representative images of cells in the clusters marked by corresponding numbers in the scatter plots. (*F*) No significant differences in lymphocyte cell size were found between healthy blood donors (*gray*, n = 24), recovered patients approximately 5 months after undergoing COVID-19 (*green*, n = 14), and patients hospitalized with COVID-19 (*yellow*, n = 17). (*G*) Lymphocytes exhibit significantly increased deformation in hospitalized COVID-19 patients. (*H*) Young's modulus of lymphocytes is significantly lower in COVID-19 patients compared with the healthy or recovered donors. Statistical comparisons were done using Kruskal-Wallis test with Dunn's post hoc test; $*p < 0.05$, $**p < 0.01$, $***p < 0.001$.

cell size did not differ among healthy donors, recovered, and hospitalized COVID-19 patients (medians 37.8 ± 1.3, 38.6 ± 0.7, and 39.0 ± 2 μm^2, respectively; Fig. 3 *F*), lymphocyte deformation in standardized channel flow conditions was elevated during COVID-19. Compared with the healthy donor median deformation 0.025 ± 0.006, hospitalized COVID-19 patient lymphocytes had a significantly higher median deformation 0.029 ± 0.003, $p = 0.011$ (Fig. 3 *G*). Lymphocyte deformation was 0.026 ± 0.002 for recovered patients, not significantly different from that of the control group.

The sphericity of lymphocytes under normal conditions allowed us to exploit the developed theoretical framework (13) to calculate the Young's modulus from RT-DC data. The Young's modulus, a measure of overall cell stiffness, was significantly lower in the COVID-19 cohort ($p = 0.003$, $\chi^2 = 11.7$, $\varepsilon^2 = 0.22$) (Fig. 3 *H*). Although the control group median Young's modulus was 1.15 ± 0.12 kPa, it went down to 1.03 ± 0.10 kPa in hospitalized COVID-19 patients ($p = 0.003$, Dunn's post hoc test), reflecting a decrease of stiffness. The decreased Young's modulus in lymphocytes during COVID-19 was further confirmed by comparing the data of three patients during and after COVID-19 (Fig. S3 *L*). To the best of our knowledge, this study reveals the first evidence of altered mechanical properties of lymphocytes during COVID-19.

Monocytes of COVID-19 patients exhibit a dramatic increase in cell volume

In inflammatory disease, monocytes can contribute to the immune response either directly or via differentiation into dendritic cells or macrophages. Therefore, it is not surprising that altered monocyte phenotype and function is characteristic for COVID-19 patients (1). Examination of monocytes with RT-DC revealed a significant change in monocyte size ($p < 0.0001$, $\chi^2 = 30.6$, $\varepsilon^2 = 0.57$) triggered by the appearance of larger monocytes during COVID-19 (Fig. 4, *A–D*). Monocytes of hospitalized COVID-19 patients had a median cell cross-sectional area of 70.5 ± 7.1 μm^2, significantly higher compared with recovered patients (65.0 ± 2.5 μm^2, $p < 0.0001$, Dunn's post hoc test) and that of the healthy cohort, 63.8 ± 2.2 μm^2 ($p < 0.0001$; Fig. 4 *E*). This represents a 9.5% increase from the median cross-sectional area of the healthy cohort. In addition, the SD of the cross-sectional area increased during COVID-19 ($p = 0.001$, $\chi^2 = 13.7$, $\varepsilon^2 = 0.25$) because of the appearance of large monocytes (Fig. 4 *F*).

The differences in cell volume were also pronounced ($p < 0.0001$, $\chi^2 = 27.7$, $\varepsilon^2 = 0.51$), with a 16.7% increase of median cell volume during COVID-19. The median volume of COVID-19 patient monocytes was 353.7 ± 55.8 μm^3 compared with 303.2 ± 12.0 μm^3 for the healthy cohort and 304.9 ± 19.4 μm^3 for recovered patients (Fig. 4 *G*). Assuming a spherical shape, this would correspond to monocyte

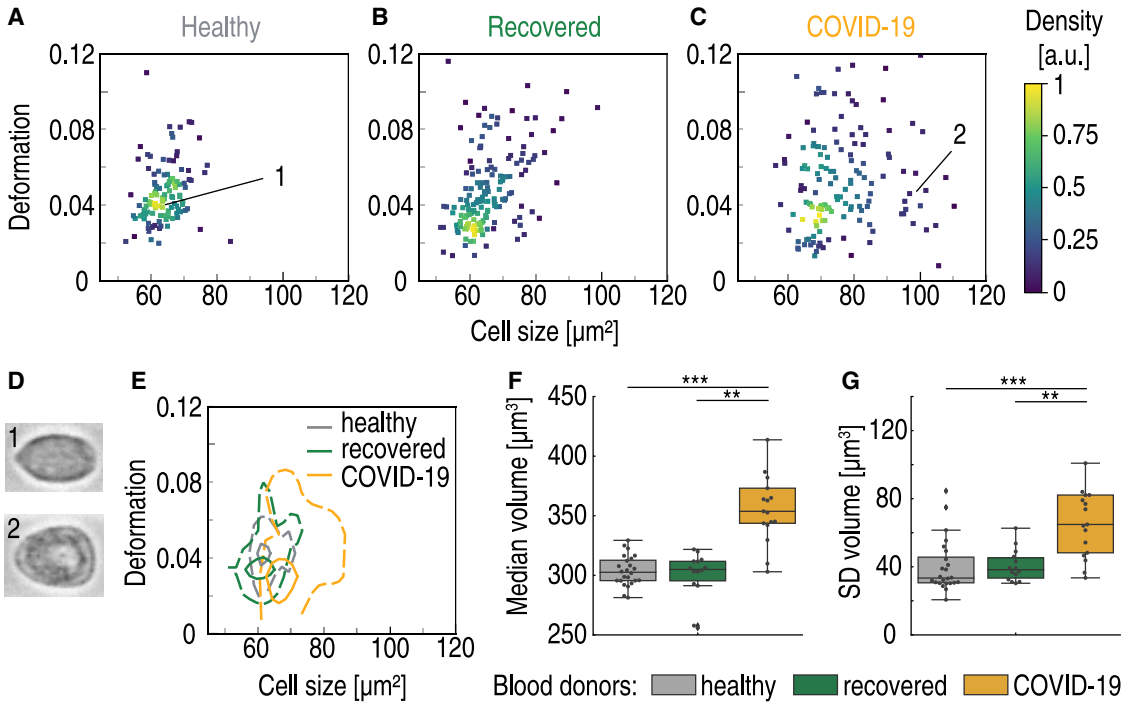

FIGURE 4 The appearance of large monocytes in COVID-19 patients. Typical scatter plot of monocyte deformation versus cell size (cross-sectional area) of a healthy blood donor with no known viral infection (*A*) compared with a patient 4 months after undergoing COVID-19 (*B*) and a patient with COVID-19 in an intensive care unit (*C*) is given. (*D*) The images of cells marked by corresponding numbers in the scatter plots. (*E*) Kernel density estimate plots demonstrating the differences in cell size and deformation among the three donors (*A–C*). (*F*) The median monocyte cell volume is significantly elevated in hospitalized COVID-19 patients (*yellow*, n = 17) compared with healthy blood donors (*gray*, n = 24) and recovered patients (*green*, n = 14). (*G*) A significant increase is also observed in the SD of cell volume. Statistical comparisons were done using Kruskal-Wallis test with Dunn's post hoc test; $*p < 0.05$, $**p < 0.01$, $***p < 0.001$.

diameters of 8.8 μm for COVID-19 patients and 8.3 μm for healthy donors. Again, the SD of the cell volume was significantly higher for COVID-19 patients ($p < 0.0001$, $\chi^2 = 18.5$, $\varepsilon^2 = 0.34$), as shown in Fig. 4 *H*. The observed size changes could be because of the appearance of a subpopulation of large, possibly highly phagocytic monocytes (28). The morphological anomaly of COVID-19 patient monocytes has been observed by Zhang et al. (29). In their study, monocyte size was assessed indirectly using flow cytometry forward scatter (FSC). Unlike RT-DC, FSC measurement does not quantify absolute size changes (30). Still, the authors were able to observe a relative change of monocyte size and reported an increase in COVID-19 compared with healthy individuals, in line with our observation. In their study, the FSC-high population was more pronounced in patients requiring hospitalization and intensive care unit admission.

No significant differences in deformation or Young's modulus were found among the three studied groups (Fig. S4), proving that the stiffness of monocytes remained unchanged during COVID-19.

Altered physical phenotype signals neutrophil activation in COVID-19

Finally, RT-DC analysis provided evidence of significant changes with strong effect sizes in neutrophil cross-sectional area ($p < 0.0001$, $\chi^2 = 23.0$, $\varepsilon^2 = 0.43$), volume ($p < 0.0001$, $\chi^2 = 23.5$, $\varepsilon^2 = 0.44$), and deformation ($p = 0.0013$, $\chi^2 = 13.3$, $\varepsilon^2 = 0.25$) (Fig. 5). During COVID-19, neutrophils were on average larger (68.7 $\pm$ 3.5 μm^2 vs. healthy donors 63.5 $\pm$ 2.2 μm^2, $p < 0.0001$), had higher volume (327.5 $\pm$ 27.2 μm^3 vs. healthy donors 292.0 $\pm$ 12.9 μm^3, $p < 0.0001$), and were more deformed under the standard capillary flow conditions in RT-DC (0.059 $\pm$ 0.009 vs. healthy donors 0.051 $\pm$ 0.004, $p = 0.002$) (Fig. 5, *F–H*). The SDs of neutrophil cross-sectional area, volume, and deformation were also significantly higher in the COVID-19 patients compared with healthy individuals (Fig. S5), reflecting higher heterogeneity in the population of neutrophils.

We hypothesize that the described changes of physical properties observed with RT-DC are linked to an activated state of neutrophils. The joint increase of size and deformation of stimulated neutrophils in vitro and in vivo has been documented by RT-DC analysis previously (9,31). Change in these parameters could serve as a proxy readout for neutrophil activation. The underlying mechanism is still unclear, although it has been reported that the volume of activated neutrophils increases through connected Na^+/H+ antiport activity (32). Our observations can also reflect the fact that in severe COVID-19, strongly activated neutrophils may adopt a so-called low-density phenotype that is

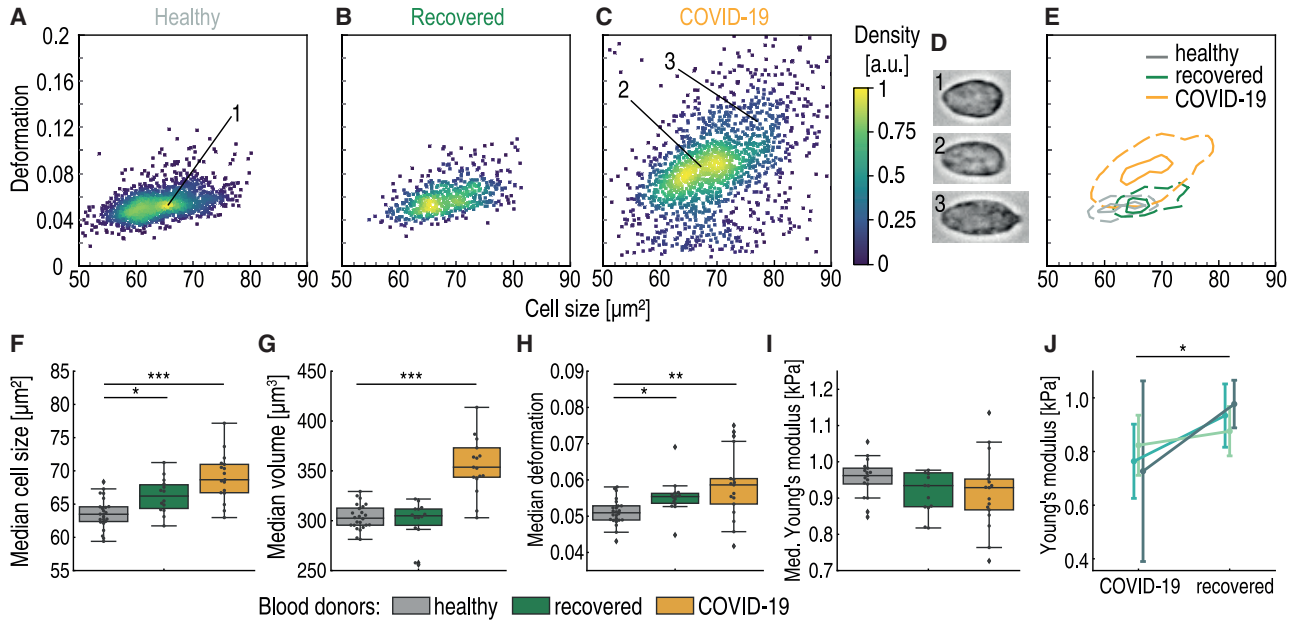

FIGURE 5 Altered physical phenotype of neutrophils in the peripheral blood of COVID-19 patients. Typical scatter plot of neutrophil deformation versus cell size (cross-sectional area) of a healthy blood donor with no known viral infection (*A*) compared with a patient 4 months after undergoing COVID-19 (*B*) and a patient with COVID-19 in an intensive care unit (*C*) is given. (*D*) Images of neutrophils marked by corresponding numbers in the scatter plots. (*E*) Kernel density estimate plots demonstrating the differences in cell size and deformation among the three donors (*A–C*). (*F*) The median cross-sectional area and (*G*) median cell volume of neutrophils of patients hospitalized with COVID-19 (*yellow*, n = 17) are significantly higher than those of the healthy blood donors (*gray*, n = 24) and of recovered patients approximately 5 months after undergoing COVID-19 (*green*, n = 14). (*H*) Neutrophils exhibit increased deformability in hospitalized COVID-19 patients compared with the healthy cohort. (*I*) Young's modulus of neutrophils of the three donor groups. (*J*) Young's modulus of neutrophils in three patients measured at two time points: during COVID-19 and after recovery. Circle markers represent the median value, and error bars represent SD. Statistical comparisons for (*F*)–(*I*) were done using Kruskal-Wallis test with Dunn's post hoc test and for (*J*) using linear mixed model analysis; $*p < 0.05$, $**p < 0.01$, $***p < 0.001$.

prone to neutrophil extracellular trap formation (33). The lower density of this population of neutrophils could be logically linked with the elevated size and deformability observed with RT-DC. The process was reported as a source of vascular occlusion, possibly leading to vascular damage and organ dysfunction in COVID-19 (33).

The median Young's modulus calculated from RT-DC data exhibited a weak decrease during COVID-19 (Fig. 5 *I*), revealing that neutrophils were generally less stiff in COVID-19 patients. These changes of Young's modulus were further confirmed by comparing data of three patients during and after COVID-19 (Fig. 5 *J*), demonstrating a clear decrease of neutrophil stiffness during COVID-19.

Interestingly, in recovered patients, neutrophil parameters (cross-sectional cell area 66.2 ± 2.5 μm^2, volume 308.9 ± 15.3 μm^3, deformation 0.055 ± 0.005) had not returned to the values of the healthy cohort (Fig. 5, *F–H*). Carissimo et al. (34) found that the neutrophil counts per defined volume of blood in recovered patients did not fully return to values of healthy individuals. Together with our findings, this suggests that COVID-19 infection leaves a lasting influence on the immune system.

In addition to neutrophils, we also examined a different group of granulocytes, eosinophils. Eosinophils are known to react to certain viral infections of the respiratory system in vitro and in vivo, including respiratory syncytial virus and influenza (35,36). However, eosinophils did not show any changes of their physical phenotype during infection or in recovered state (Fig. S6).

The earlier described findings were reported as the medians and SDs of three mostly independent cohorts of blood donors. For three of the patients, we performed RT-DC measurements both during COVID-19 and after recovery and could therefore directly examine the progression of blood cell parameters in a single individual. The comparison of various blood cell features of these three donors at the two studied time points can be found in Figs. S2–S6. The trends confirm what we describe in the text earlier; severe COVID-19 is linked with the presence of erythrocytes with distinct phenotype and lower deformation, larger monocytes, softer lymphocytes, and larger, more deformed neutrophils.

DISCUSSION

In our study, the physical parameters of blood cells, including mechanical properties, act as sensitive reporters of pathophysiological changes in COVID-19 patients compared with age-matched controls. The concept that cell morphology and mechanics are inherent markers of cell function has long been established (37,38). Using RT-DC,

we were able to monitor the physical properties of cells from whole blood without the need for tedious preparation or enrichment. In COVID-19 patients, we found alterations of erythrocytes and leukocyte subsets with the potential to be exploited as diagnostic markers. This paves the way for high-speed, label-free, and cost-effective disease detection. We note that the relatively low number of COVID samples included in our study and the huge space of possible cellular responses to viral infection makes it a necessity to acquire many more RT-DC data sets to ensure the specificity of an observed pattern for a particular disease. In the context of limited existing RT-DC data on viral infections, the blood cell response to COVID-19 was unique. In a previous study, neutrophils derived from patients with viral respiratory tract (RTI) and EBV infection exhibited similar changes in cell size and deformation as those we observed for COVID-19 (9). In RTI and EBV, monocytes were larger and significantly more deformable than the controls, whereas in COVID-19, monocyte deformation did not change. Lymphocytes showed distinct responses to the three viral infections: in COVID-19 they were more deformable, in RTI they showed no changes, and in EBV the lymphocytes were bigger and more deformable compared with controls (9). In the future, RT-DC could be of high significance for the fast identification of a specific infection of viral or other origin. This would be an advantage in times when molecular diagnostic tests such as qPCR become inaccessible, such as during critical phases of a pandemic.

A key finding of our study was that the erythrocytes of COVID-19 patients were significantly more heterogeneous in size and deformation under constant shear stress compared with healthy controls. In a recent report, Thomas et al. (25) identified structural protein damage and membrane lipid remodeling in erythrocytes as potential causes of impaired oxygen delivery during COVID-19. These changes could be linked with the altered physical properties of the cells, as the composition and properties of plasma membranes interplay with the cytoskeleton to regulate physical properties of cells such as shape (39). The physical properties of erythrocytes are crucial for microcirculatory flow (40,41), and as such, these changes could impair circulation and promote hypoxemia. The effect could persist in COVID-19 patients long after the infection was not active anymore; we found that in recovered patients, phenotype alterations were not as prominent but still present. A different explanation for the persistence of less deformable erythrocytes in recovered patients could be that the cells already had a different physical phenotype before clinical onset. Altered mechanical properties of cells because of factors such as age could increase susceptibility to SARS-CoV-2 infection, as suggested by Uhler and Shivashankar (42).

Although erythrocytes are present in high quantities (three orders of magnitude more frequent than leukocytes), the numbers and physical features of leukocytes are also crucial for proper blood flow (43). RT-DC provides direct access to relative leukocyte counts, their size, and mechanical properties. In accordance with other studies (18,19), we found neutrophilia and lymphopenia as well as increased NLR in COVID-19 patients. Importantly, we report on changes of size and mechanical properties of leukocyte subsets in COVID-19 samples. These changes might be key to understanding vessel occlusion and pulmonary embolism, as the interrogation of cell morphology and mechanics in former studies established the importance of these factors for cell circulation under physical (44), pathological (45,46), and artificial (47) conditions.

We hypothesize that the observed changes could arise because of cytoskeletal alterations of immune cells. Mechanical properties of cells can be directly related to the cytoskeleton (37,38,48,49), an important supportive structure that also determines cellular function (50–53). Previously, RT-DC allowed us to detect actin cytoskeletal rearrangements during rubella virus infection, which correlated with an altered cell shape and reduced migratory potential (54). Although it is known that viruses can use immune cells as vehicles to travel the body (55) and hijack the actin cytoskeleton (56), viral traces were absent in the blood of COVID-19 patients (57). However, the cytoskeleton may be affected by the infection indirectly, e.g., through the involvement of cytoskeleton-dependent signaling (58). Hyperinflammation and cytokine storm syndrome are reported in COVID-19 cases with high levels of macrophage inflammatory protein 1-α, granulocyte-colony stimulating factor (G-CSF), interleukins IL-2 and IL-7, interferon-γ inducible protein 10, monocyte chemoattractant protein 1, and tumor necrosis factor-α (TNF) (59). Such cytokines were reported to induce cytoskeletal changes in myeloid cells and to interfere with their physical phenotypes during immune function (60–62). For example, Kutsuna et al. (60) found actin depolymerization and changes of cell morphology upon treating neutrophils with TNF, G-CSF, and granulocyte-macrophage colony-stimulating factor (GM-CSF), suggesting cell softening. In an RT-DC study, GM-CSF was found to activate neutrophils and induce similar size and deformation changes to what we have seen for neutrophils from COVID-19 patients (31). This leads us to speculate on the possible role of cytokines in triggering cytoskeletal reorganization and physical changes of immune cells during COVID-19.

We are aware of certain limitations of our study, e.g., that it falls short of representative patient cohorts to compare mild with critical symptoms. Still, we were able to identify changes of blood cell physical phenotypes that did not return to the baseline healthy donor levels several months after SARS-CoV-2 infection, namely in erythrocytes and neutrophils. It is important to mention that neutrophils are short lived cells with an average lifespan of less than 1 day. Thus, neutrophil alterations observed in our recovered cohort were induced after the successful displacement of

the virus by the immune system. This might be indicative for SARS-CoV-2 causing long-term immunological signals or even targeting bone marrow stem cells, as viral RNA was found postmortem in patient bone marrow (63).

The persistent alterations of erythrocytes and neutrophils could be connected with long-term symptoms of the recovered patients, of which 70% described chronic headache or neurological symptoms, 54% had concentration disorders, and 62% circulatory problems such as cold sweat and tachycardia. We hypothesize that the persisting changes of blood cell physical phenotypes could contribute to the long-term impairment of circulation and oxygen delivery linked with COVID-19 (17).

Finally, we would like to add a speculative thought on cell physical changes as a tightly regulated mechanism by which the body controls the circulation or extravasation of immune cells. Fay et al. (44) reported in 2016 that cellular softening mediates leukocyte demargination and trafficking, thereby increasing clinical blood counts. It is possible that in similar manner, cell size contributes to the effective cell circulation. If a cell is smaller or more deformable, it could circulate better through narrow capillaries compared with a bigger or stiffer one. Thus, precise cell size or mechanics adaptations could control the retention of leukocytes in tissue capillaries and subsequently lead to extravasation.

Taken together, label-free physical phenotyping of blood cells with RT-DC provides a fast, sensitive, and unbiased way to feel for functional changes in cells. As such, deformability cytometry data have the potential to be used as a biomarker of COVID-19 and potentially other infectious diseases. In the future, RT-DC could be part of the first line of defense against an unknown virus during a pandemic.

SUPPORTING MATERIAL

Supporting material can be found online at https://doi.org/10.1016/j.bpj.2021.05.025.

AUTHOR CONTRIBUTIONS

M.Kubánková, J.G., and M.Kräter designed the project outline and carried out experiments, interpreted results, and wrote the initial manuscript. B.H. and M.H. provided samples and patient information, interpreted and discussed results, and co-wrote the manuscript. J.H. and J.F. provided samples and patient information and co-wrote the manuscript.

ACKNOWLEDGMENTS

The authors thank Leonie Staats and Aylin Lindemann for technical assistance and Despina Soteriou, Michael Moritz, Charlotte Szewczykowski, and Folkert Horn for study support.

REFERENCES

1. Mann, E. R., M. Menon, …, T. Hussell; NIHR Respiratory TRC; CIRCO. 2020. Longitudinal immune profiling reveals key myeloid signatures associated with COVID-19. *Sci. Immunol.* 5:eabd6197.
2. Tay, M. Z., C. M. Poh, …, L. F. P. Ng. 2020. The trinity of COVID-19: immunity, inflammation and intervention. *Nat. Rev. Immunol.* 20:363–374.
3. Mehta, P., D. F. McAuley, …, J. J. Manson; HLH Across Speciality Collaboration, UK. 2020. COVID-19: consider cytokine storm syndromes and immunosuppression. *Lancet.* 395:1033–1034.
4. Tang, N., D. Li, …, Z. Sun. 2020. Abnormal coagulation parameters are associated with poor prognosis in patients with novel coronavirus pneumonia. *J. Thromb. Haemost.* 18:844–847.
5. Chen, N., M. Zhou, …, L. Zhang. 2020. Epidemiological and clinical characteristics of 99 cases of 2019 novel coronavirus pneumonia in Wuhan, China: a descriptive study. *Lancet.* 395:507–513.
6. Di Carlo, D. 2012. A mechanical biomarker of cell state in medicine. *J. Lab. Autom.* 17:32–42.
7. Lipowsky, H. H. 2005. Microvascular rheology and hemodynamics. *Microcirculation.* 12:5–15.
8. Otto, O., P. Rosendahl, …, J. Guck. 2015. Real-time deformability cytometry: on-the-fly cell mechanical phenotyping. *Nat. Methods.* 12:199–202, 4 p after 202.
9. Toepfner, N., C. Herold, …, J. Guck. 2018. Detection of human disease conditions by single-cell morpho-rheological phenotyping of blood. *eLife.* 7:e29213.
10. Müller, P., E. O'Connell, and M. Schlögel. 2019. Shape-Out version 2.3.0: Graphical user interface for analysis and visualization of RT-DC data sets. GitHub https://github.com/ZELLMECHANIK-DRESDEN/ShapeOut2.
11. Müller, P., E. O'Connell, M. Herbig, M. Schlögel, and P. Rosendahl. 2015. dclab version 0.31.2: Python library for the post-measurement analysis of real-time deformability cytometry data sets. GitHub https://github.com/ZELLMECHANIK-DRESDEN/dclab.
12. Mokbel, M., D. Mokbel, …, S. Aland. 2017. Numerical simulation of real-time deformability cytometry to extract cell mechanical properties. *ACS Biomater. Sci. Eng.* 3:2962–2973.
13. Mietke, A., O. Otto, …, E. Fischer-Friedrich. 2015. Extracting cell stiffness from real-time deformability cytometry: theory and experiment. *Biophys. J.* 109:2023–2036.
14. Kelley, T. L. 1935. An unbiased correlation ratio measure. *Proc. Natl. Acad. Sci. USA.* 21:554–559.
15. Tomczak, M., and E. Tomczak. 2014. The need to report effect size estimates revisited. An overview of some recommended measures of effect size. *Trends Sport Sci.* 1:19–25.
16. Rea, L. M., and R. A. Parker. 2014. Designing and Conducting Survey Research: A Comprehensive Guide. Wiley, Hoboken, NJ.
17. Herbig, M., A. Mietke, …, O. Otto. 2018. Statistics for real-time deformability cytometry: clustering, dimensionality reduction, and significance testing. *Biomicrofluidics.* 12:042214.
18. Wang, D., B. Hu, …, Z. Peng. 2020. Clinical characteristics of 138 hospitalized patients with 2019 novel coronavirus-infected pneumonia in Wuhan, China. *JAMA.* 323:1061–1069.
19. Tan, L., Q. Wang, …, H. Miao. 2020. Lymphopenia predicts disease severity of COVID-19: a descriptive and predictive study. *Signal Transduct. Target. Ther.* 5:33.
20. Woodruff, M. C., R. P. Ramonell, …, I. Sanz. 2020. Extrafollicular B cell responses correlate with neutralizing antibodies and morbidity in COVID-19. *Nat. Immunol.* 21:1506–1516.
21. Liu, Y., X. Du, …, Y. Zhao. 2020. Neutrophil-to-lymphocyte ratio as an independent risk factor for mortality in hospitalized patients with COVID-19. *J. Infect.* 81:e6–e12.
22. Mei, Y., S. E. Weinberg, …, P. Ji. 2020. Risk stratification of hospitalized COVID-19 patients through comparative studies of laboratory results with influenza. *EClinicalMedicine.* 26:100475.
23. Foy, B. H., J. C. T. Carlson, …, J. M. Higgins. 2020. Association of red blood cell distribution width with mortality risk in hospitalized adults with SARS-CoV-2 infection. *JAMA Netw. Open.* 3:e2022058.
24. Della Rocca, D. G., M. Magnocavallo, …, A. Natale. 2021. Evidence of systemic endothelial injury and microthrombosis in hospitalized

COVID-19 patients at different stages of the disease. *J. Thromb. Thrombolysis.* 51:571–576.

25. Thomas, T., D. Stefanoni, …, A. D'alessandro. 2020. Evidence of structural protein damage and membrane lipid remodeling in red blood cells from COVID-19 patients. *J. Proteome Res.* 19:4455–4469.
26. Huisjes, R., A. Bogdanova, …, R. van Wijk. 2018. Squeezing for life - properties of red blood cell deformability. *Front. Physiol.* 9:656.
27. Weerahandi, H., K. A. Hochman, …, L. Horwitz. 2020. Post-discharge health status and symptoms in patients with severe COVID-19. *Prepr. Serv. Heal. Sci* 646, 501.
28. Wang, S. Y., K. L. Mak, …, C. K. Ho. 1992. Heterogeneity of human blood monocyte: two subpopulations with different sizes, phenotypes and functions. *Immunology.* 77:298–303.
29. Zhang, D., R. Guo, …, J. Hu. 2021. Frontline science: COVID-19 infection induces readily detectable morphologic and inflammation-related phenotypic changes in peripheral blood monocytes. *J. Leukoc. Biol.* 109:13–22, Published online October 11, 2020.
30. Nawaz, A. A., M. Urbanska, …, J. Guck. 2020. Intelligent image-based deformation-assisted cell sorting with molecular specificity. *Nat. Methods.* 17:595–599.
31. Bashant, K. R., A. Vassallo, …, N. Toepfner. 2019. Real-time deformability cytometry reveals sequential contraction and expansion during neutrophil priming. *J. Leukoc. Biol.* 105:1143–1153.
32. Hayashi, H., O. Aharonovitz, …, S. Grinstein. 2008. Na^+/H^+ exchange and pH regulation in the control of neutrophil chemokinesis and chemotaxis. *Am. J. Physiol. Cell Physiol.* 294:C526–C534.
33. Leppkes, M., J. Knopf, …, M. Herrmann. 2020. Vascular occlusion by neutrophil extracellular traps in COVID-19. *EBioMedicine.* 58:102925.
34. Carissimo, G., W. Xu, …, L. F. Ng. 2020. Whole blood immunophenotyping uncovers immature neutrophil-to-VD2 T-cell ratio as an early marker for severe COVID-19. *Nat. Commun.* 11:5243.
35. Phipps, S., C. En Lam, …, K. I. Matthaei. 2007. Eosinophils contribute to innate antiviral immunity and promote clearance of respiratory syncytial virus. *Blood.* 110:1578–1586.
36. Flores-Torres, A. S., M. C. Salinas-Carmona, …, A. G. Rosas-Taraco. 2019. Eosinophils and respiratory viruses. *Viral Immunol.* 32:198–207.
37. Fletcher, D. A., and R. D. Mullins. 2010. Cell mechanics and the cytoskeleton. *Nature.* 463:485–492.
38. Kasza, K. E., A. C. Rowat, …, D. A. Weitz. 2007. The cell as a material. *Curr. Opin. Cell Biol.* 19:101–107.
39. Diz-Muñoz, A., D. A. Fletcher, and O. D. Weiner. 2013. Use the force: membrane tension as an organizer of cell shape and motility. *Trends Cell Biol.* 23:47–53.
40. Lanotte, L., J. Mauer, …, M. Abkarian. 2016. Red cells' dynamic morphologies govern blood shear thinning under microcirculatory flow conditions. *Proc. Natl. Acad. Sci. USA.* 113:13289–13294.
41. Reichel, F., J. Mauer, …, D. A. Fedosov. 2019. High-throughput microfluidic characterization of erythrocyte shapes and mechanical variability. *Biophys. J.* 117:14–24.
42. Uhler, C., and G. V. Shivashankar. 2020. Mechano-genomic regulation of coronaviruses and its interplay with ageing. *Nat. Rev. Mol. Cell Biol.* 21:247–248.
43. Qiu, Y., D. R. Myers, and W. A. Lam. 2019. The biophysics and mechanics of blood from a materials perspective. *Nat. Rev. Mater.* 4:294–311.
44. Fay, M. E., D. R. Myers, …, W. A. Lam. 2016. Cellular softening mediates leukocyte demargination and trafficking, thereby increasing clinical blood counts. *Proc. Natl. Acad. Sci. USA.* 113:1987–1992.
45. Rosenbluth, M. J., W. A. Lam, and D. A. Fletcher. 2008. Analyzing cell mechanics in hematologic diseases with microfluidic biophysical flow cytometry. *Lab Chip.* 8:1062–1070.
46. Lam, W. A., M. J. Rosenbluth, and D. A. Fletcher. 2008. Increased leukaemia cell stiffness is associated with symptoms of leucostasis in paediatric acute lymphoblastic leukaemia. *Br. J. Haematol.* 142:497–501.
47. Tietze, S., M. Kräter, …, J. Guck. 2019. Spheroid culture of mesenchymal stromal cells results in morphorheological properties appropriate for improved microcirculation. *Adv. Sci. (Weinh.).* 6:1802104.
48. Bausch, A. R., and K. Kroy. 2006. A bottom-up approach to cell mechanics. *Nat. Phys.* 2:231–238.
49. Pegoraro, A. F., P. Janmey, and D. A. Weitz. 2017. Mechanical properties of the cytoskeleton and cells. *Cold Spring Harb. Perspect. Biol.* 9:a022038.
50. Szymanski, D., and C. J. Staiger. 2018. The actin cytoskeleton: functional arrays for cytoplasmic organization and cell shape control. *Plant Physiol.* 176:106–118.
51. Fais, S., F. Luciani, …, F. Lozupone. 2000. Linkage between cell membrane proteins and actin-based cytoskeleton: the cytoskeletal-driven cellular functions. *Histol. Histopathol.* 15:539–549.
52. Etienne-Manneville, S. 2004. Actin and microtubules in cell motility: which one is in control? *Traffic.* 5:470–477.
53. Pollard, T. D., and G. G. Borisy. 2003. Cellular motility driven by assembly and disassembly of actin filaments. *Cell.* 112:453–465.
54. Kräter, M., J. Sapudom, …, C. Claus. 2018. Alterations in cell mechanics by actin cytoskeletal changes correlate with strain-specific rubella virus phenotypes for cell migration and induction of apoptosis. *Cells.* 7:136.
55. Fackler, O. T., T. T. Murooka, …, T. R. Mempel. 2014. Adding new dimensions: towards an integrative understanding of HIV-1 spread. *Nat. Rev. Microbiol.* 12:563–574.
56. Döhner, K., and B. Sodeik. 2005. The role of the cytoskeleton during viral infection. *Curr. Top. Microbiol. Immunol.* 285:67–108.
57. Wölfel, R., V. M. Corman, …, C. Wendtner. 2020. Virological assessment of hospitalized patients with COVID-2019. *Nature.* 581:465–469.
58. Janmey, P. A. 1998. The cytoskeleton and cell signaling: component localization and mechanical coupling. *Physiol. Rev.* 78:763–781.
59. Huang, C., Y. Wang, …, B. Cao. 2020. Clinical features of patients infected with 2019 novel coronavirus in Wuhan, China. *Lancet.* 395:497–506.
60. Kutsuna, H., K. Suzuki, …, S. Kitagawa. 2004. Actin reorganization and morphological changes in human neutrophils stimulated by TNF, GM-CSF, and G-CSF: the role of MAP kinases. *Am. J. Physiol. Cell Physiol.* 286:C55–C64.
61. Girard, D., M. E. Paquet, …, A. D. Beaulieu. 1996. Differential effects of interleukin-15 (IL-15) and IL-2 on human neutrophils: modulation of phagocytosis, cytoskeleton rearrangement, gene expression, and apoptosis by IL-15. *Blood.* 88:3176–3184.
62. Bashant, K. R., N. Toepfner, …, E. R. Chilvers. 2020. The mechanics of myeloid cells. *Biol. Cell.* 112:103–112.
63. Deinhardt-Emmer, S., D. Wittschieber, …, G. Mall. 2021. Early postmortem mapping of SARS-CoV-2 RNA in patients with COVID-19 and the correlation with tissue damage. *eLife.* 10:e60361.

Biophysical Journal, Volume *120*

Supplemental information

Physical phenotype of blood cells is altered in COVID-19

Markéta Kubánková, Bettina Hohberger, Jakob Hoffmanns, Julia Fürst, Martin Herrmann, Jochen Guck, and Martin Kräter

Physical phenotype of blood cells is altered in COVID-19

M Kubánková, B Hohberger, J Hoffmanns, J Fürst, M Herrmann, J Guck[#], M Kräter

corresponding author

1

Supplementary Figures and Tables

Supplementary table 1. Patient characteristics, medical management and outcome of all donors included in this study.

	All donors n=54 (100%)		
	Control n=24	**Recovered n=14**	**COVID-19 n=17**
Age (years): median (range)	62.5 ± 13.6 years (26-81)	58.6 ± 12.4 (27-76)	68·± 10.4 (41-87)
Gender			
male	12 (50%)	10 (71.4%)	13 (76.5%)
female	12 (50%)	4 (18.6%)	4 (23.5%)
Primary virus identification (PCR airway)	n.a.	14 (100%)	17 (100%)
Complications and medical management			
Oxygen supplementation	0	0	17 (100%)
Mechanical ventilation	0	0	13 (76.5%)
ECMO	0	0	6 (35.3%)
Dialysis	0	0	3 (17.6%)
Systemic Superinfection	0	0	7 (41.1%)
Pulmonary embolism	0	0	6 (35.3%)
Drugs			
Azithromycin	0	0	3 (17.6%)
Hydroxychloroquine	0	0	9 (52.9%)
Heparin prophylactic/therapeutic anticoagulation	0	0	13 (76.5%)
Outcome			
Length of hospital stay (days)	0	7 ± 2.4 (5-12)	22.8 ± 14 (7-50)
Intensive care unit stay	0	0	13 (76.5%)
Discharged	0	14 (100%)	9 (52.9%)
Further hospitalized	0	0	0
Death	0	0	8 (47.1%)

Supplementary table 2. Kruskal-Wallis *H*-statistics, *p*-values and effect sizes ε^2. The last three columns represent *p*-values from Dunn's posthoc tests conducted for the significant results of Kruskal-Wallis *H*-tests.

A - healthy B- recovered C - COVID	*p* (Kruskal-Wallis)	*H* (Kruskal-Wallis)	ε^2 (Kruskal-Wallis)	*p* AC (Dunn's)	*p* AB (Dunn's)	*p* BC (Dunn's)
Erythrocytes						
Median area	0.1162	4.30	0.080	0.4896	0.1503	1.0000
SD area	0.0000	26.99	0.500	0.0000	0.2259	0.0112
Median volume	0.2532	2.75	0.051	1.0000	0.2938	1.0000
SD volume	0.0000	33.75	0.625	0.0000	0.9204	0.0002
Median deformation	0.2180	3.05	0.056	0.4480	1.0000	0.3380
SD deformation	0.0000	42.30	0.783	0.0000	0.0024	0.0340
% of ery with def < 0.28	0.0000	25.83	0.478	0.0000	1.0000	0.0016
Neutrophils						
Median area	0.0000	22.95	0.425	0.0000	0.2704	0.0260
SD area	0.0001	18.86	0.349	0.0023	0.0001	0.6791
Median volume	0.0000	23.53	0.436	0.0000	0.1319	0.0517
SD volume	0.0001	19.78	0.366	0.0005	0.0002	1.0000
Median deformation	0.0013	13.31	0.246	0.0021	1.0000	0.0319
SD deformation	0.0059	10.28	0.190	0.0041	0.3772	0.5059
Median Young's modulus	0.1698	3.55	0.066	0.1827	1.0000	0.8807
Lymphocytes						
Median area	0.0499	6.00	0.111	0.1667	1.0000	0.0939
SD area	0.0000	30.78	0.570	0.2270	0.0010	0.0000
Median volume	0.0814	5.02	0.093	0.3403	1.0000	0.1134
SD volume	0.0000	28.36	0.525	0.7403	0.0003	0.0000
Median deformation	0.0132	8.66	0.160	0.0107	0.1945	1.0000
SD deformation	0.0000	35.61	0.659	0.0043	0.0218	0.0000
Median Young's modulus	0.0029	11.68	0.216	0.0029	0.0542	1.0000
Monocytes						
Median area	0.0000	30.64	0.567	0.0000	0.0001	1.0000
SD area	0.0011	13.65	0.253	0.0007	0.0892	0.7682
Median volume	0.0000	27.71	0.513	0.0000	0.0001	1.0000
SD volume	0.0001	18.48	0.342	0.0001	0.0075	1.0000
Median deformation	0.7918	0.47	0.009	1.0000	1.0000	1.0000
SD deformation	0.4949	1.41	0.026	0.7256	1.0000	1.0000
Median Young's modulus	0.7763	0.51	0.009	1.0000	1.0000	1.0000
Eosinophils						
Median area	0.1289	4.10	0.076	0.6099	0.1547	1.0000
SD area	0.0126	8.7600	0.162	0.1245	0.0168	1.0000
Median volume	0.2532	2.75	0.051	1.0000	0.2938	1.0000
SD volume	0.0000	33.75	0.625	0.0000	0.9204	0.0002
Median deformation	0.4143	1.76	0.033	1.0000	0.9095	0.5981
SD deformation	0.5965	1.03	0.019	1.0000	1.0000	0.9290
Median Young's modulus	0.9592	0.08	0.002	1.0000	1.0000	1.0000
% of WBC						
% neutrophils	0.0105	9.10	0.169	0.0499	1.0000	0.0174
% lymphocytes	0.0007	14.63	0.271	0.0006	0.2426	0.0328
% monocytes	0.0151	8.38	0.155	0.0244	1.0000	0.0644
% eosinophils	0.0010	13.73	0.254	0.1576	0.0007	0.1970
NLR	0.0022	12.22	0.226	0.0031	0.7018	0.0252

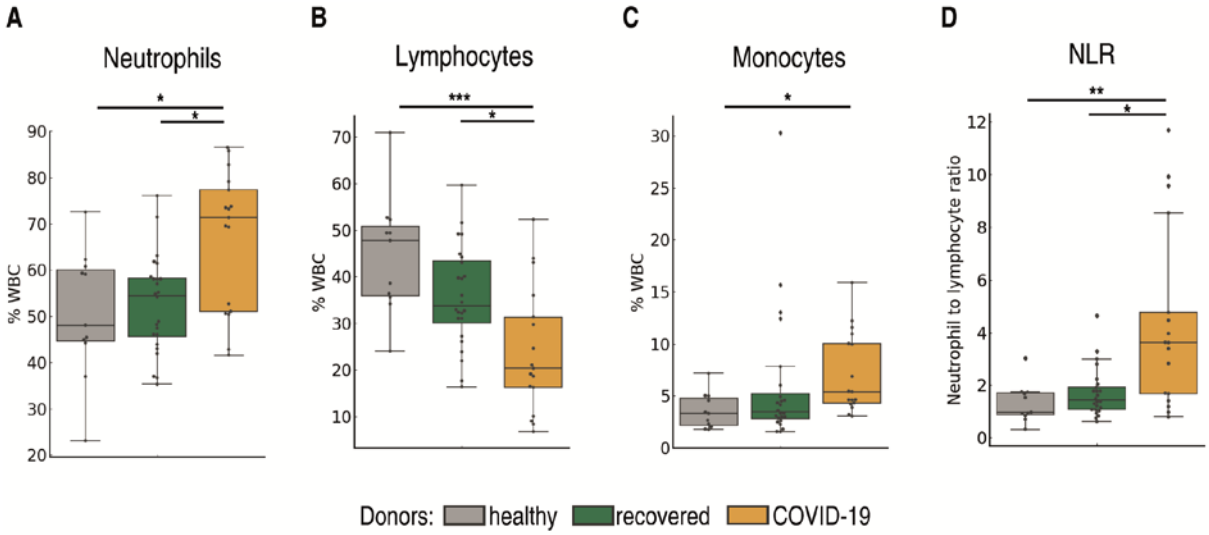

Supplementary figure 1. Proportions of white blood cells calculated from real-time deformability cytometry (RT-DC) data. The percentage of A) neutrophils, B) lymphocytes and C) monocytes in the total white blood cell count; a comparison of the control blood donor cohort (grey), recovered patients (green) and hospitalized COVID-19 patients (yellow). D) The neutrophil to lymphocyte ratio is significantly higher in hospitalized patients compared to the recovered and healthy donor cohorts, * $p < .05$, ** $p < .01$, *** $p < .001$.

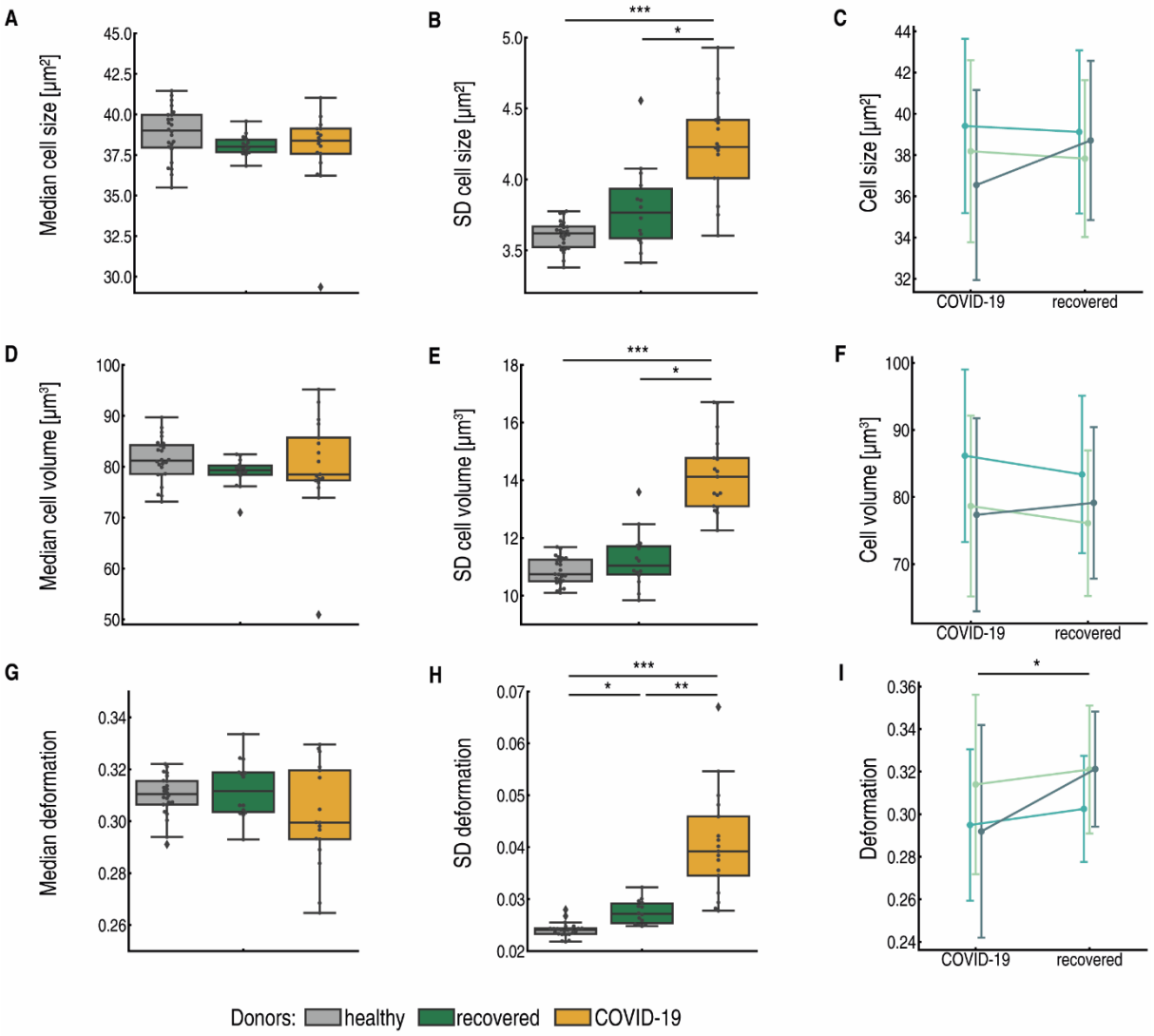

Supplementary figure 2. Physical properties of erythrocytes of COVID-19 patients compared to controls. Quantification of A-C) cross-sectional cell area, D-F) cell volume, G-I) cell deformation; in these graphs COVID-19 patients (yellow, n = 17) are compared to recovered donors (green, n = 14) and healthy donors (grey, n = 24). Panels C), F), I) show three patients measured at two time points, during COVID-19 and after recovery; circle markers represent the median value and error bars represent the standard deviation for each patient. Statistical comparisons in C), F), I) were performed using linear mixed model analysis. All other statistical comparisons were done using Kruskal-Wallis test with Dunn's posthoc test. * $p < .05$, ** $p < .01$, *** $p < .001$.

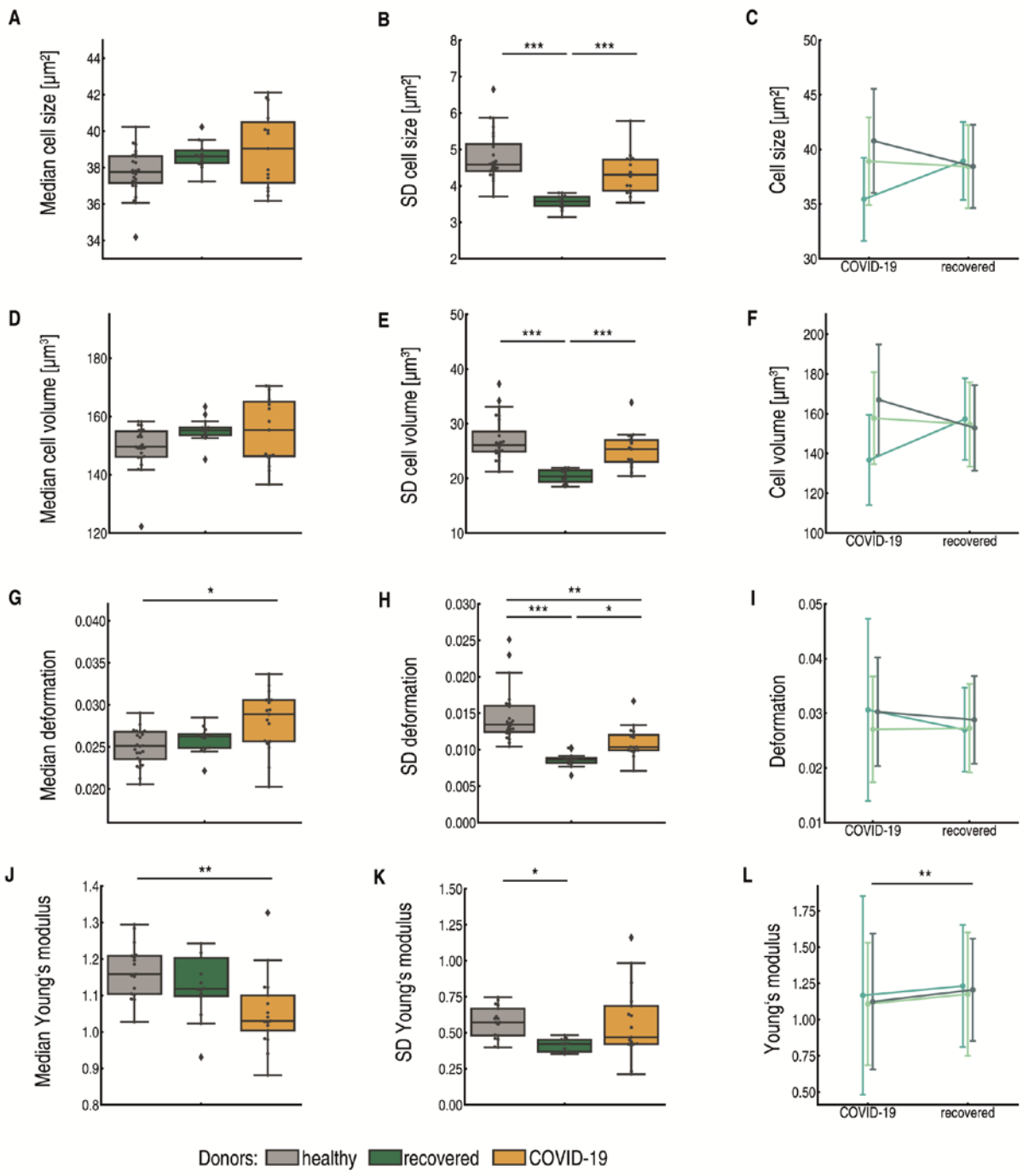

Supplementary figure 3. Physical properties of lymphocytes of COVID-19 patients compared to controls. Quantification of A-C) cross-sectional cell area, D-F) cell volume, G-I) cell deformation, J-L) Young's modulus; in these graphs COVID-19 patients (yellow, n = 17) are compared to recovered donors (green, n = 14) and healthy donors (grey, n = 24). Panels C), F), I) and L) show three patients measured at two time points, during COVID-19 and after recovery; circle markers represent the median value and error bars represent the standard deviation for each patient. Statistical comparisons in C), F), I), L) were performed using linear mixed model analysis. All other statistical comparisons were done using Kruskal-Wallis test with Dunn's posthoc test. * $p < .05$, ** $p < .01$, *** $p < .001$.

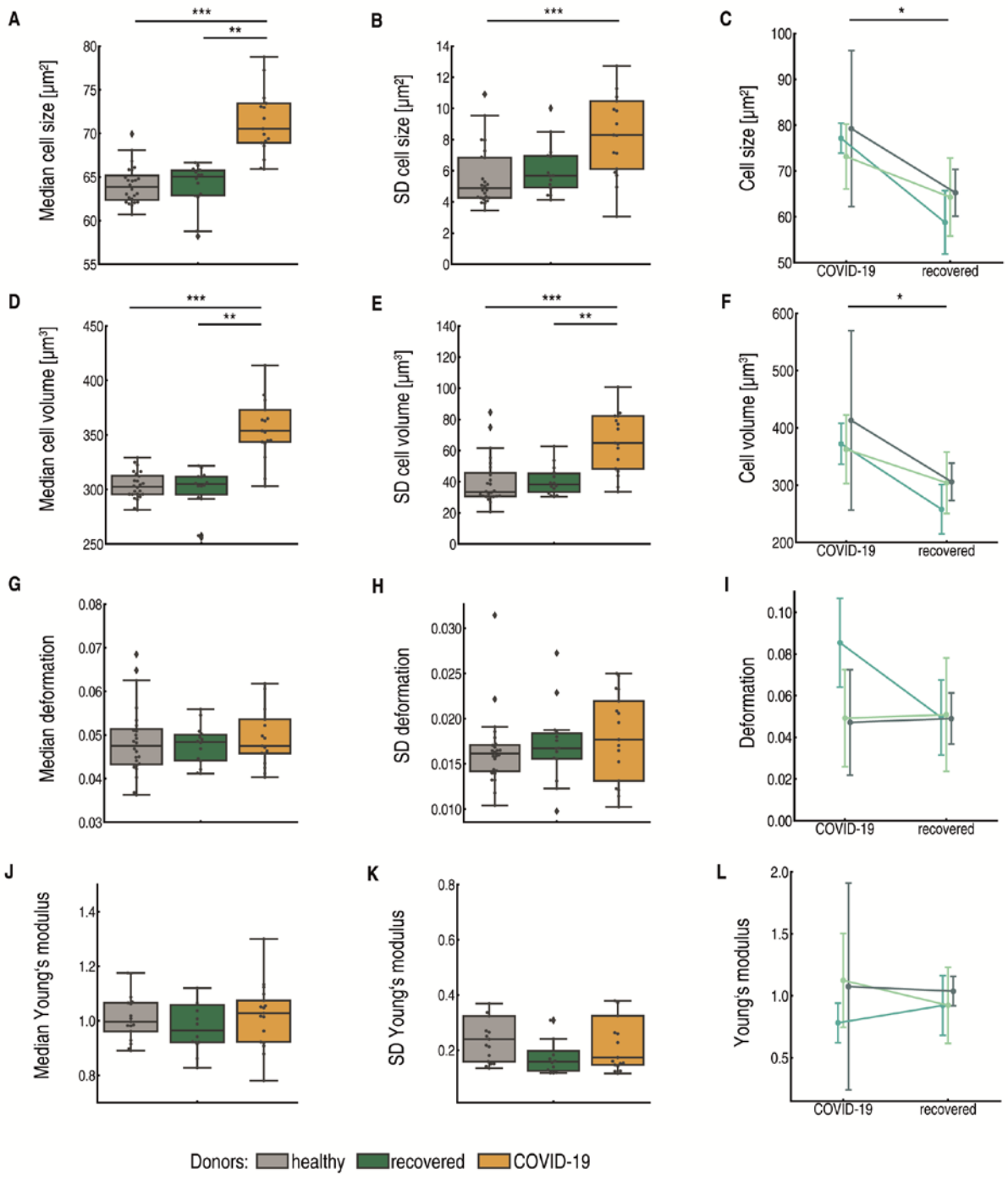

Supplementary figure 4. Physical properties of monocytes of COVID-19 patients compared to controls. Quantification of A-C) cross-sectional cell area, D-F) cell volume, G-I) cell deformation, J-L) Young's modulus; in these graphs COVID-19 patients (yellow, n = 17) are compared to recovered donors (green, n = 14) and healthy donors (grey, n = 24). Panels C), F), I) and L) show three patients measured at two time points, during COVID-19 and after recovery; circle markers represent the median value and error bars represent the standard deviation for each patient. Statistical comparisons in C), F), I), L) were performed using linear mixed model analysis. All other statistical comparisons were done using Kruskal-Wallis test with Dunn's posthoc test. * $p < .05$, ** $p < .01$, *** $p < .001$.

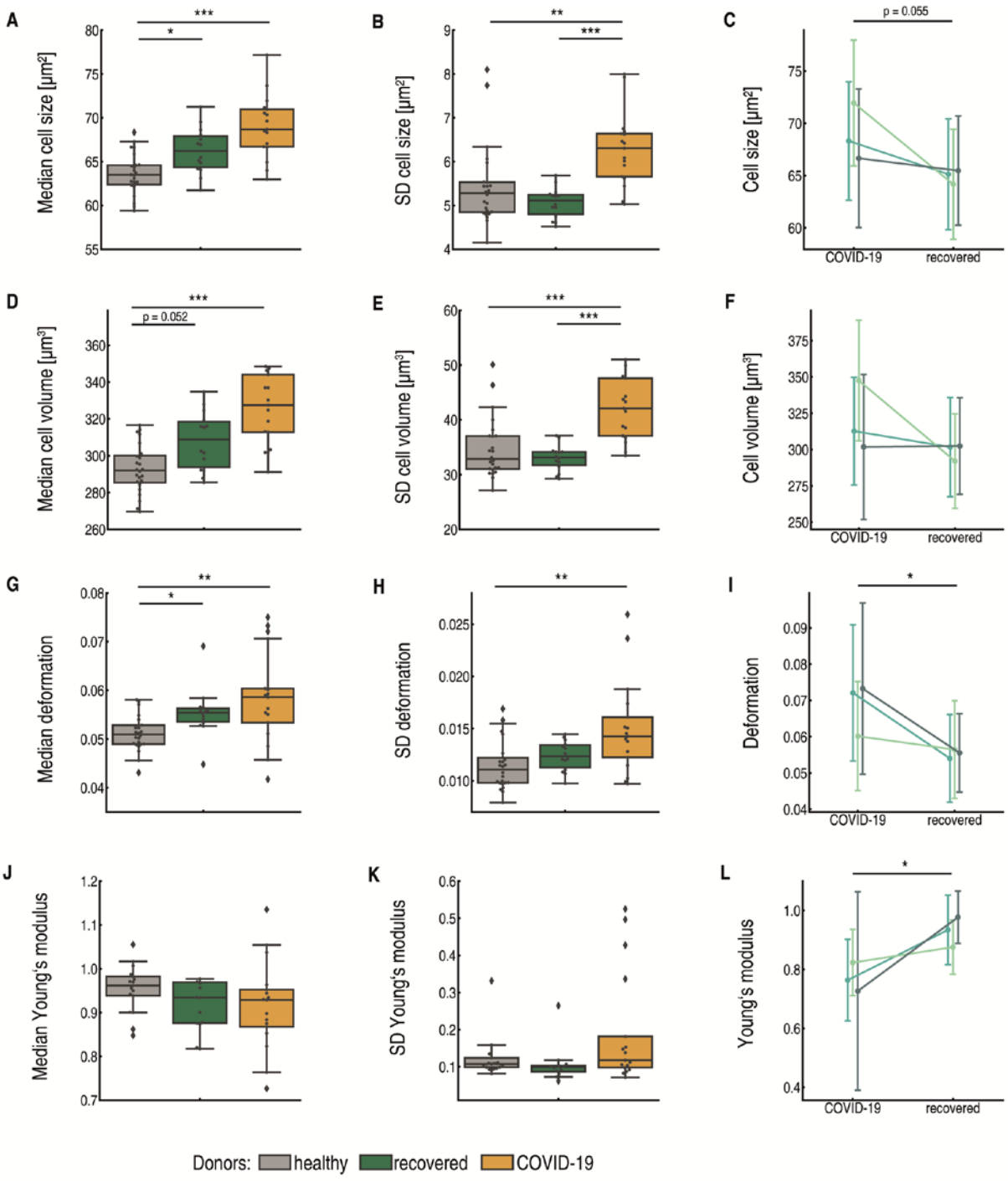

Supplementary figure 5. Physical properties of neutrophils of COVID-19 patients compared to controls. Quantification of A-C) cross-sectional cell area, D-F) cell volume, G-I) cell deformation, J-L) Young's modulus; in these graphs COVID-19 patients (yellow, n = 17) are compared to recovered donors (green, n = 14) and healthy donors (grey, n = 24). Panels C), F), I) and L) show three patients measured at two time points, during COVID-19 and after recovery; circle markers represent the median value and error bars represent the standard deviation for each patient. Statistical comparisons in C), F), I), L) were performed using linear mixed model analysis. All other statistical comparisons were done using Kruskal-Wallis test with Dunn's posthoc test. * $p < .05$, ** $p < .01$, *** $p < .001$.

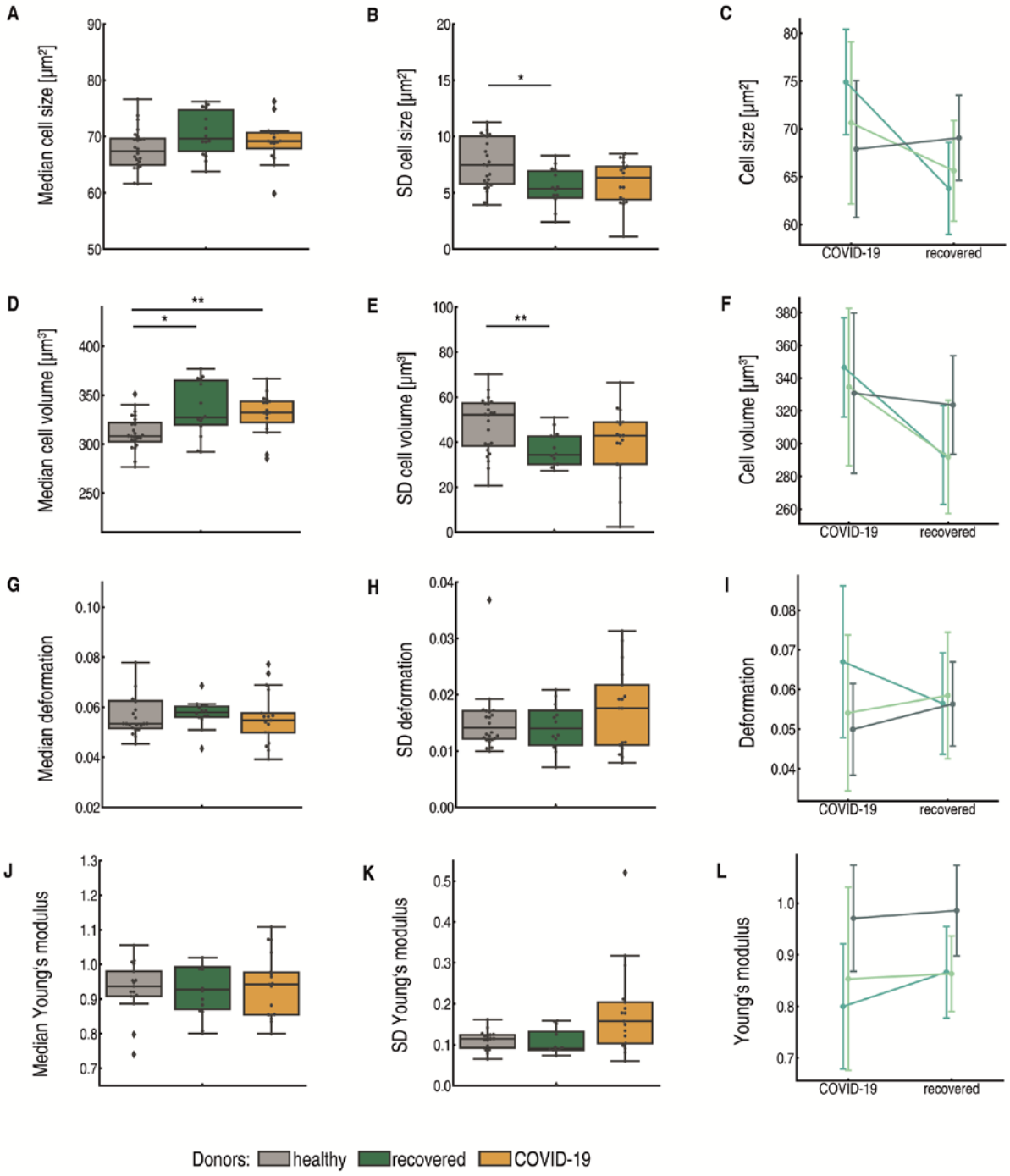

Supplementary figure 6. Physical properties of eosinophils of COVID-19 patients compared to controls. Quantification of A-C) cross-sectional cell area, D-F) cell volume, G-I) cell deformation, J-L) Young's modulus; in these graphs COVID-19 patients (yellow, n = 17) are compared to recovered donors (green, n = 14) and healthy donors (grey, n = 24). Panels C), F), I) and L) show three patients measured at two time points, during COVID-19 and after recovery; circle markers represent the median value and error bars represent the standard deviation for each patient. Statistical comparisons in C), F), I), L) were performed using linear mixed model analysis. All other statistical comparisons were done using Kruskal-Wallis test with Dunn's posthoc test. * $p < .05$, ** $p < .01$, *** $p < .001$.

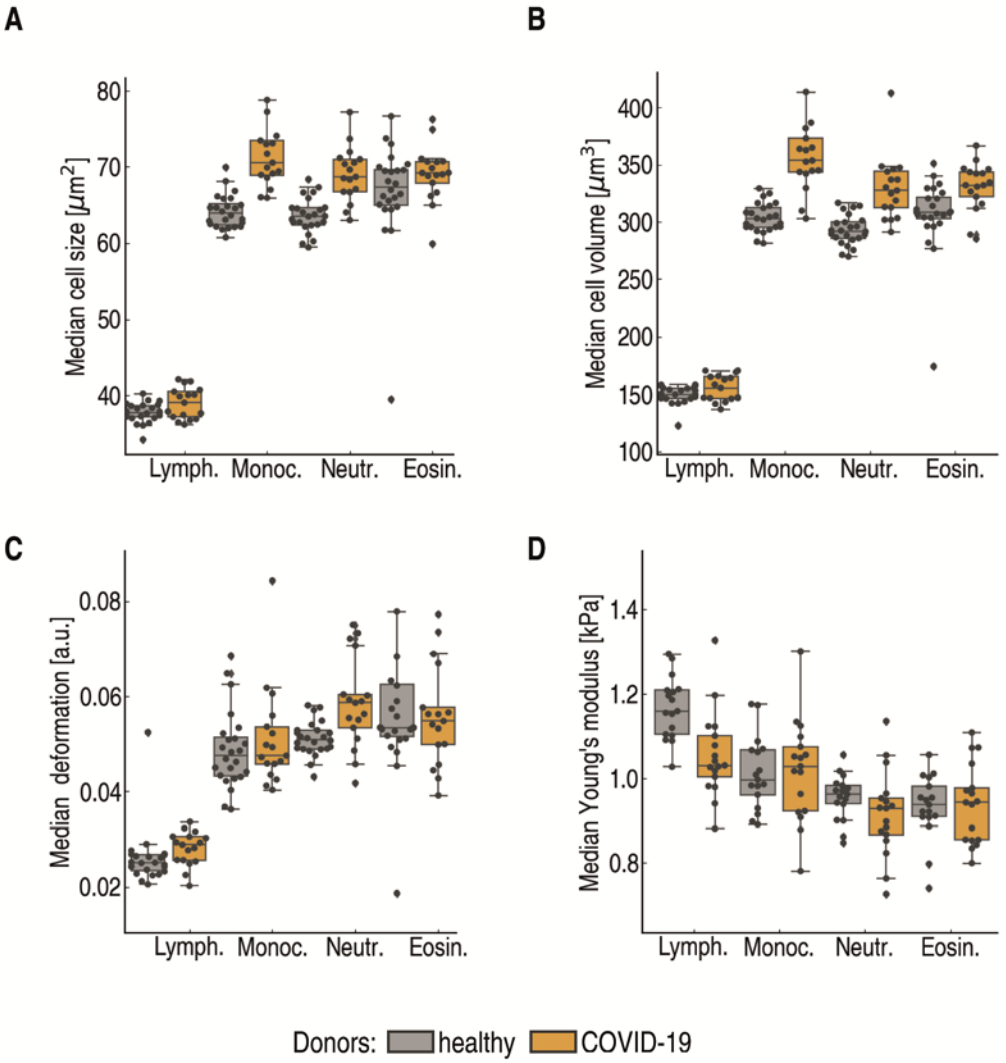

59

60 **Supplementary figure 7. A comparison of the physical properties of the four examined white blood**
61 **cell types in COVID-19 patients (yellow) compared to the control group (grey).** A) Median cell size, B)
62 median cell volume, C) median deformation, D) median Young's modulus.